JOURNAL OF GEOPHYSICAL RESEARCH, VOL. 95, NO. D6, PAGES 7467-7483, MAY 20, 1990

Two-Dimensional Atmospheric Transport and Chemistry Model: Numerical Experiments With a New Advection Algorithm

RUN-LIE SHIA, YUK LUNG HA, JUN-SHAN WEN, AND YUK L. YUNG

Division of Geological and Planetary Sciences, California Institute of Technology, Pasadena

Extensive testing of the advective scheme, proposed by Prather (1986), has been carried out in support of the California Institute of Technology–Jet Propulsion Laboratory two-dimensional model of the middle atmosphere. We generalize the original scheme to include higher-order moments. In addition, we show how well the scheme works in the presence of chemistry as well as eddy diffusion. Six types of numerical experiments including simple clock motion and pure advection in two dimensions have been investigated in detail. By comparison with analytic solutions it is shown that the new algorithm can faithfully preserve concentration profiles, has essentially no numerical diffusion, and is superior to a typical fourth-order finite difference scheme.

INTRODUCTION

In one-dimensional photochemical models of the stratosphere (for example, *Logan et al.* [1978]) transport is parameterized by eddy diffusion. Numerical simulation of a diffusive process is generally straightforward and stable. With the advent of two-dimensional photochemical models (see, for example, *Garcia and Solomon* [1983]) advection becomes the dominant mode of transport, with eddy diffusion playing a minor role. Numerical modeling of advection, unlike that of diffusion, is extremely difficult. The most simple and straightforward schemes based on centered differencing are grossly inadequate. The principal shortcomings of these schemes are numerical diffusion and dispersion [*Rood*, 1987]. Dispersion usually generates unacceptable negative concentrations of a tracer. The problems with numerical diffusion are more subtle. For example, any attempt to correct the unphysical situation of negative concentrations by "borrowing and filling" results in artificial diffusion, which may be confused with the real physical diffusion. This is serious because most current two-dimensional models [*Garcia and Solomon*, 1983; *Guthrie et al.*, 1984; *Ko et al.*, 1985] adopt low values for the horizontal eddy diffusivity, $K_{yy} \sim 10^9$ cm^2 s^{-1}. According to *Ko et al.* [1985], the choice of such low K_{yy} requires an accurate advective algorithm so that the "numerical diffusion" does not overwhelm the real diffusion. An accurate algorithm is necessary for simulating transport of a tracer with large spatial gradients, such as the impulsive insertion of a tracer after a nuclear explosion or volcanic eruption. An extensive review of advective algorithms and their role in atmospheric transport and chemical models has been carried out by *Rood* [1987]. The method we adopt for the California Institute of Technology–Jet Propulsion Laboratory (Caltech–JPL) two-dimensional model is due to *Prather* [1986], based on the conservation of moments. It is mentioned only briefly in Rood's comprehensive review. We note that most advection schemes [*Haltiner and Williams*, 1980; *Rood*, 1987] are based on finite differences. Prather's scheme is fundamentally different because it uses an integral approach, which can explicitly include additional information about the tracer distribution within each grid box at each time step. Partly because of this, the time step can be close to the Courant limit. The high accuracy with low numerical dispersion and diffusion achieved by this method is also due to the additional information stored at each time step (conservation of second-order moments requires carrying six moments in two dimensions, whereas a finite difference scheme usually stores only the concentration, which is proportional to the zeroth moment).

We have carried out extensive testing of the Prather method in support of the development of our two-dimensional model. The original Prather scheme was formulated for pure advection on a Cartesian grid. We have modified the algorithm to account for the sphericity of the atmosphere and to include eddy diffusion and chemistry. We have made six types of numerical experiments to validate our model by comparing the results with analytic solutions, if they exist, and, in some experiments, with the numerical results using a fourth-order Arakawa scheme [*Arakawa*, 1966]. This scheme conserves the total mass of the tracer, $\sum_{i,j} \chi_{i,j}$, as well as the sum of mass squared, $\sum_{i,j} \chi_{i,j}^2$ (for details, see Appendix B), and is one of the best fourth-order finite difference schemes.

The complete list of numerical experiments is summarized in Table 1. Experiments 1 and 2 are intended to test the performance of the Prather scheme in a two-dimensional Cartesian grid for wind velocities that correspond to rigid body rotation and rotation with constant angular velocity shear, respectively. Experiments 3 and 4 are designed to test the Prather scheme in problems involving eddy diffusion and chemistry in addition to advection. Experiment 5 tests the Prather scheme for performance under pure advection on an altitude-latitude grid. This case closely simulates actual stratospheric transport. Finally, experiment 6 is an attempt to generalize the scheme to higher-order moments beyond the second. As will be shown, in all cases tested, Prather's algorithm consistently yielded higher quality simulations with low numerical diffusion and dispersion. The last experiment shows that there is not much to be gained by going to higher moments.

Paper number 89JD01616.
0148-0227/90/89JD-01616$05.00

TABLE 1. List of Numerical Experiments Performed to Test the Accuracy of Prather's Advection Scheme in Our Two-Dimensional Tracer Model

	Experiment	Type of Grid	Specifications and Remarks
1a	rigid body rotation	2-D Cartesian	40 × 40 grid Initial distribution = elliptical cone centered at the origin
1b	same as above	same as 1a	same as above, except Initial distribution = off-centered square column
2	rotation with constant angular velocity shear	same as 1a	same as above, except Initial distribution = off-centered circular cone
3a	flow with diffusion + chemistry	restricted 2-D	1 latitude layer × 16 altitude layers, steady state; advection dominated
3b	same as 3a	same as 3a	1 latitude layer × 8 altitude layers; steady state; diffusion dominated
3c	same as 3a	same as 3a	same as above, except chemistry dominated
4	advection with chemistry	2-D latitude × altitude	19 × 17 grid, steady state
5	a more realistic advection	2-D latitude × altitude	30 × 15 grid, steady state
6	conservation of higher moments	1-D	10, 20, and 40 grid boxes, no chemistry

Abbreviations are 2-D, two dimensional; 1-D, one dimensional.

MECHANISTIC STRUCTURE OF THE TWO-DIMENSIONAL MODEL FOR TRACE SPECIES

The meridional coordinate adopted in the Caltech–JPL two-dimensional model is $y = a\theta$, where a is planetary radius, and θ is latitude defined to be $-\pi/2$ at the South Pole and $\pi/2$ at the North Pole. For vertical coordinate we choose $z = H \ln (p_s/p)$, where p is pressure, p_s is surface pressure, and H is a fixed constant. The constants p_s and H are set equal to 1000 mbar and 8 km, respectively, in this paper. We also use the dimensionless coordinate $\xi = z/H$. The stream function ψ for the residual mean circulation is computed from net heating rates or may be entered directly for specialized calculations. From the stream function we can readily derive velocities for meridional motion v and vertical motion w,

$$v = -\frac{1}{\cos\theta} e^{\xi} \frac{\partial}{\partial z} \left(e^{-\xi}\psi\right) \tag{1}$$

$$w = \frac{1}{\cos\theta} \frac{\partial \psi}{\partial y} \tag{2}$$

This velocity field $\mathbf{u} = (v, w)$ is nondivergent in the following sense:

$$e^{\xi} \nabla \cdot \left(e^{-\xi}\mathbf{u}\right) = \frac{1}{\cos\theta} \frac{\partial}{\partial y}(\cos\theta v) + e^{\xi} \frac{\partial}{\partial z} \left(e^{-\xi} w\right) = 0 \tag{3}$$

The eddy diffusive fluxes are parameterized by

$$F_y = -\left(K_{yy} \frac{\partial \chi}{\partial y} + K_{yz} \frac{\partial \chi}{\partial z}\right) \tag{4}$$

$$F_z = -\left(K_{zy} \frac{\partial \chi}{\partial y} + K_{zz} \frac{\partial \chi}{\partial z}\right) \tag{5}$$

where χ is the mixing ratio of the tracer under consideration. The eddy diffusivity tensor K_{ij} cannot be arbitrarily specified but must be derived self-consistently with the adopted advection [*Tung*, 1987]. The continuity equation for the mixing ratio of a trace species is

$$\frac{\partial \chi}{\partial t} + v \frac{\partial \chi}{\partial y} + w \frac{\partial \chi}{\partial z} - \frac{1}{\cos\theta} \frac{\partial}{\partial y} \left\{\cos\theta \left(K_{yy} \frac{\partial \chi}{\partial y} + K_{yz} \frac{\partial \chi}{\partial z}\right)\right\}$$

$$- e^{\xi} \frac{\partial}{\partial z} \left\{e^{-\xi} \left(K_{zy} \frac{\partial \chi}{\partial y} + K_{zz} \frac{\partial \chi}{\partial z}\right)\right\} = \frac{1}{M}(P - L) \tag{6a}$$

where P is rate of chemical production per unit volume, L is rate of chemical loss per unit volume, and M is the number density of the ambient atmosphere. The right-hand side of (6a) denotes the time rate of change of χ, the divergence of advective fluxes, and the divergence of diffusive fluxes (F_i). In practice, we prefer to compute with an equivalent equation using the stream function rather than the velocities,

$$\frac{\partial \chi}{\partial t} - \frac{1}{\cos\theta} \left[e^{\xi} \frac{\partial}{\partial z}(e^{-\xi}\psi) \frac{\partial \chi}{\partial y} - \frac{\partial \psi}{\partial y} \frac{\partial \chi}{\partial z}\right]$$

$$- \frac{1}{\cos\theta} \frac{\partial}{\partial y} \left\{\cos\theta \left(K_{yy} \frac{\partial \chi}{\partial y} + K_{yz} \frac{\partial \chi}{\partial z}\right)\right\}$$

$$- e^{\xi} \frac{\partial}{\partial z} \left\{e^{-\xi} \left(K_{zy} \frac{\partial \chi}{\partial y} + K_{zz} \frac{\partial \chi}{\partial z}\right)\right\}$$

$$= \frac{1}{M}(P - L) \tag{6b}$$

To solve this equation numerically, we divide the atmosphere into $N_y \times N_z$ boxes. An example of a hypothetical model atmosphere with $N_y = 5$ and $N_z = 6$ is shown in Figure 1. Note that the mean mixing ratio χ is defined at the center of each grid box. The stream function ψ is defined at the corners of the grid boxes so that differentiation of ψ, approximated by finite difference, can produce the appropriate advective velocities. This procedure guarantees mass conservation within each grid box without further adjustment (see Appendix A). The locations of other important physical quantities are as indicated in this figure. To compute diffusive fluxes, the usual centered finite difference procedure is used. The natural boundary conditions at the poles are zero horizontal fluxes. This is guaranteed by a proper choice of the stream function and by imposing zero diffusive fluxes.

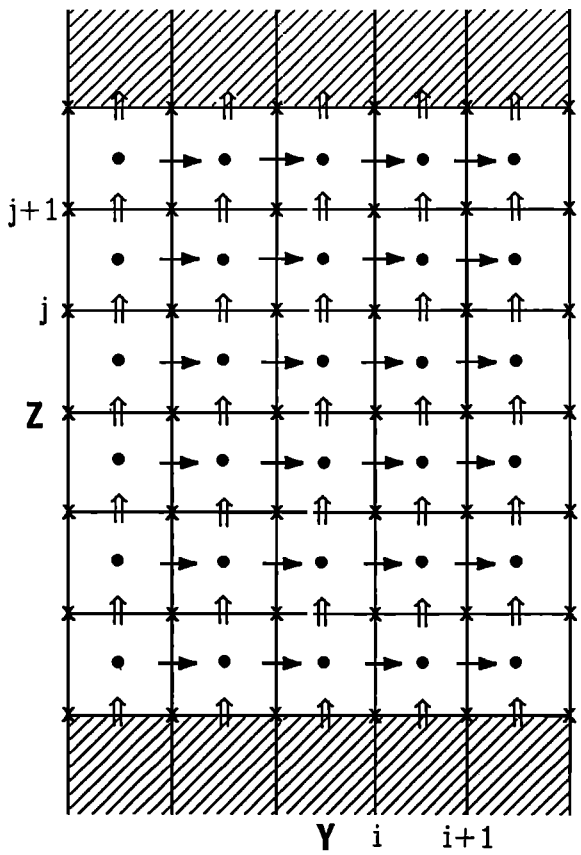

Fig. 1. A schematic two-dimensional model with five horizontal layers ($N_y = 5$) and six vertical layers ($N_z = 6$). Special symbols in the figure indicate locations where various physical quantities are defined: crosses, stream function (ψ); solid dots, mixing ratio (χ) and production (P) and loss (L) rates; horizontal arrow, horizontal velocity (v) and horizontal flux (F_y); vertical arrow, vertical velocity (w) and vertical flux (F_z).

We allow material to enter and leave the lower and upper boundaries as fluxes. In the case of imposing a fixed mixing ratio at the boundary, we create an infinitely massive layer so that a finite amount of material can flow in or out without affecting the value of the mixing ratio at the boundary.

EXPERIMENT 1: RIGID BODY ROTATION

Numerical experiments with rigid body rotation, or clock motion, have been carried out by *Molenkamp* [1968] using a number of finite difference schemes. Here we propose to investigate how faithfully the gradients of a tracer are preserved under rotation. The main advantage of this type of numerical experiments is the existence of analytic solutions. The stream function chosen for this study is, in Cartesian coordinates,

$$\psi_1(y,z) = \frac{1}{2}r^2\Omega \tag{7}$$

where

$$r = \left((y-y_o)^2 + (z-z_o)^2\right)^{\frac{1}{2}}$$

with the center of rotation located at (y_o, z_o) and Ω is the angular velocity. The corresponding meridional and vertical velocities are given by

$$v = -(z-z_o)\Omega \tag{8}$$

$$w = (y-y_o)\Omega \tag{9}$$

This motion is equivalent to rigid body rotation (or clock motion). In the numerical experiments we chose $y_o = z_o = 0$. The analytic solution for mixing ratio is

$$\chi(y,z,t) = \chi_o(y',z') \tag{10}$$

where $\chi_o(y,z)$ is the initial tracer distribution, and

$$y' = r\cos\theta' \tag{11}$$

$$z' = r\sin\theta' \tag{12}$$

$$\theta' = \theta - \Omega t \tag{13}$$

$$\theta = \tan^{-1}\left(\frac{z}{y}\right) \tag{14}$$

$$\theta' = \tan^{-1}\left(\frac{z'}{y'}\right) \tag{15}$$

In experiment 1a we chose $\Omega = 1$, and the initial tracer distribution was an elliptical cone centered at the origin,

$$\begin{aligned} \chi_o(y,z) &= 1 - \frac{r_1}{16} \quad r_1 \le 16 \\ \chi_o(y,z) &= 0 \qquad\quad r_1 > 16 \end{aligned} \tag{16}$$

where $r_1 = \left(y^2 + 4z^2\right)^{1/2}$. The model was run on a 40×40 grid for a total time of 6π (three full rotations) with time step $\Delta t = \pi/60$. The results for $t = 0$, π, 3π, and 6π are shown in Figure 2. We note that the concentration gradients are faithfully preserved by Prather's scheme at all times. For comparison we repeated this experiment with a modified fourth-order Arakawa scheme [*Arakawa*, 1966], which conserves the total mass of the tracer, $\sum_i \chi_i$, as well as the sum of mass squared, $\sum_i \chi_i^2$ (for details of our modifications, see Appendix B). The results are shown in Figure 3. It can be concluded that the Arakawa scheme is not as accurate as the Prather scheme in preserving the concentration gradients. We expect the performance of other fourth-order advection schemes to be similar to that of the Arakawa scheme and hence less accurate than Prather's scheme.

Experiment 1b is the same as experiment 1a except for the choice of initial tracer distribution, which was an off-centered square column,

$$\begin{aligned} &\chi_o(y,z) = 1 \quad 5 \le y \le 15 \quad \text{and} \quad |z| < 5 \\ &\chi_o(y,z) = 0 \quad \text{otherwise} \end{aligned} \tag{17}$$

Figures 4*a* through 4*d* present the results obtained using Prather's scheme, and Figures 5*a* through 5*d* give corresponding results obtained using Arakawa's scheme. The contrasts between the two sets of results are obvious and again demonstrate the superiority of Prather's scheme in maintaining discontinuities, sharp edges, and flat tops.

EXPERIMENT 2: ROTATION WITH CONSTANT ANGULAR VELOCITY SHEAR

In the previous numerical experiments, the "clock" motion is characterized by a constant angular velocity. In the

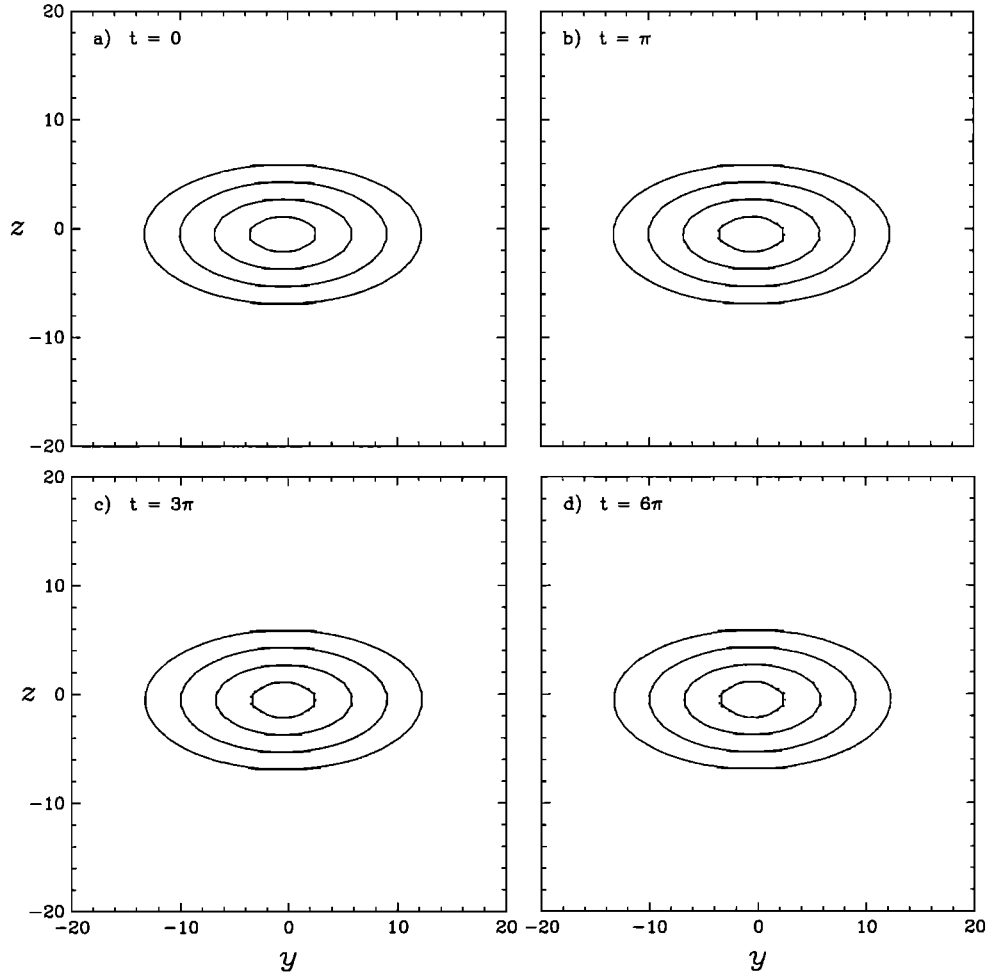

Fig. 2. Time sequence of experiment 1a with rigid body rotation at angular velocity $\Omega = 1$ centered at $(0,0)$: (*a*) $t = 0$, (*b*) $t = \pi$, (*c*) $t = 3\pi$, and (*d*) $t = 6\pi$. The grid used is Cartesian 40×40, $\Delta t = \pi/60$. Numerical solution is given by the solid lines; analytic solution by the dotted lines. The algorithm used for computing advection is Prather's scheme.

following experiments we relax this constraint and add angular velocity shear. The purpose is to test the performance of our numerical scheme when the contour lines are "stretched." The stream function is given by

$$\psi_2(y,z) = \frac{1}{3}A\Omega r^3 \tag{18}$$

where the symbols have been defined in (7), and A is a constant. The corresponding velocities are

$$v = -A\Omega(z - z_o)r \tag{19}$$

$$w = A\Omega(y - y_o)r \tag{20}$$

The analytic solution is similar to (10),

$$\chi(y,z,t) = \chi_o(y',z') \tag{21}$$

where

$$y' = r\cos\theta' \tag{22}$$

$$z' = r\sin\theta' \tag{23}$$

$$\theta' = \theta - A\Omega r t \tag{24}$$

In our experiment we assumed an initial distribution equal to an off-centered cone,

$$\begin{aligned} \chi_o(y,z) &= 1 - \frac{r_2}{8} \quad \text{for} \quad r_2 \le 8 \\ \chi_o(y,z) &= 0 \qquad\quad \text{for} \quad r_2 > 8 \end{aligned} \tag{25}$$

where $r_2 = \left[(y-10)^2 + z^2\right]^{1/2}$. The constant $A\Omega$ was set equal to unity. A much smaller time step, $\Delta t = 0.002$, was used in this experiment because of the large velocities present near the boundaries of the model. The grid was the same as in experiment 1. The results of our run with Prather's scheme are shown in Figure 6. Owing to the presence of large velocity shear, the initial distribution given by the cone was stretched into a banana-shaped object at $t = 0.38$. Figure 7 shows similar results obtained using Arakawa's scheme and demonstrates that Prather's algorithm is superior, if only marginally, to that of Arakawa.

EXPERIMENT 3: ONE-DIMENSIONAL FLOW WITH DIFFUSION AND CHEMISTRY

A realistic model for atmospheric tracers has both diffusion and chemistry in addition to pure advection. *Prather*

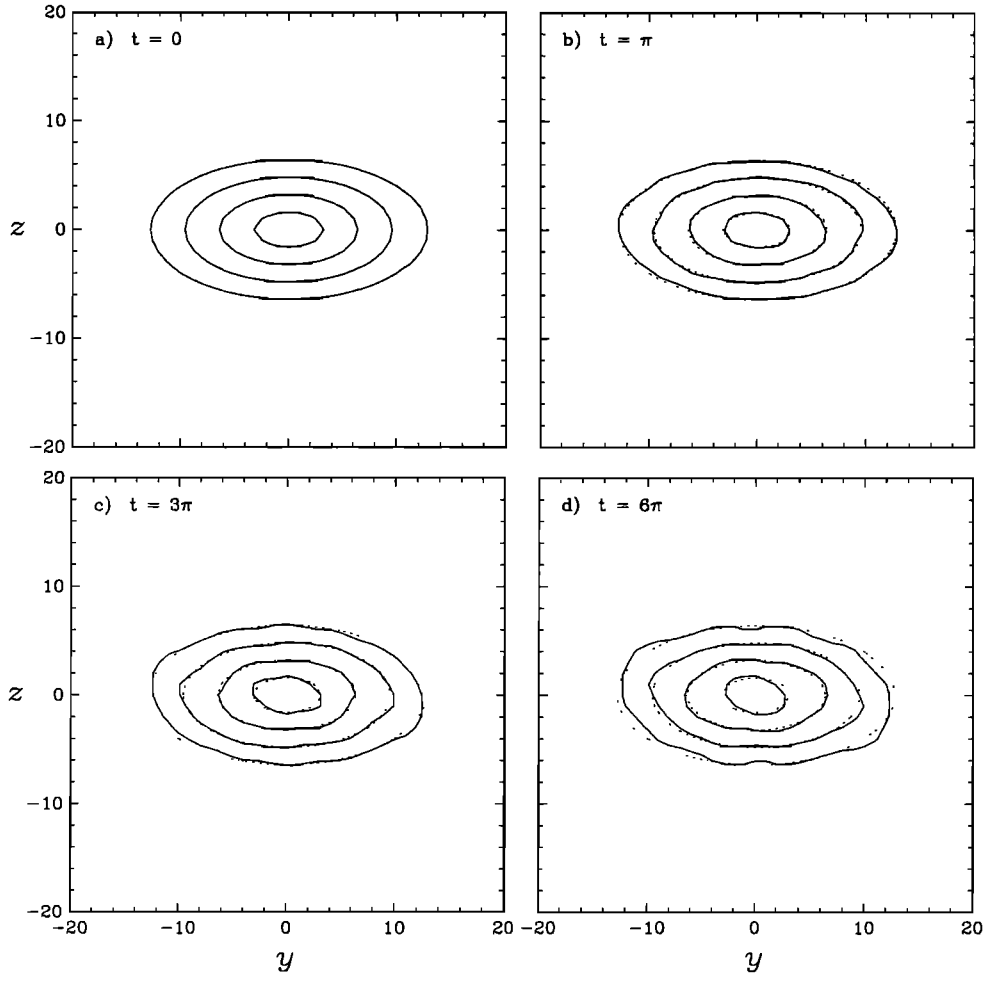

Fig. 3. Same as Figure 2, using the modified Arakawa fourth-order scheme.

[1986] did not test the performance of his scheme in the presence of diffusion and chemistry. Since the scheme deals with motion in x and y separately by time splitting, it is straightforward to add diffusion and chemistry by further time splitting. Centered differencing is used for computing diffusion. Chemistry introduces a slight complication because we do not know how all the moments respond to chemical production or loss. For simplicity, we compute the effect of chemistry on the zeroth moment (the total mass in a box) and scale all the other moments accordingly. To compute transport due to diffusion, we assume that the mean mixing ratio (proportional to the zeroth moment) refers to the center of each grid box. The usual finite-differencing scheme for computing gradient of mixing ratio is employed. We will test this procedure against an analytic solution to find out how accurate it is.

Consider the simple case of one-dimensional flow with diffusion and chemistry. The equation in steady state is, from (6a),

$$w\frac{\partial \chi}{\partial z} - e^{\xi}\frac{\partial}{\partial z}\left(e^{-\xi}K_{zz}\frac{\partial \chi}{\partial z}\right) = \frac{1}{M}(P - L) \tag{26}$$

where the flow velocity w must be nondivergent, that is,

$$e^{\xi}\frac{\partial}{\partial z}\left(e^{-\xi}w\right) = 0 \tag{27}$$

A simple choice of w that satisfies the above condition is

$$w = w_o e^{\xi} \tag{28}$$

In order to derive an analytic solution, we assume

$$K_{zz} = K_o e^{\xi} \tag{29}$$

$$P = P_o e^{\alpha \xi} \tag{30}$$

$$L = L_o M e^{\xi}\chi \tag{31}$$

where $M = M_o e^{-\xi}$, and α is a constant. Introducing dimensionless variables,

$$\omega = \frac{w_o H}{K_o} \tag{32}$$

$$s = \frac{P_o H^2}{M_o K_o} \tag{33}$$

$$\ell = \frac{L_o H^2}{K_o} \tag{34}$$

the continuity equation becomes

$$\frac{d^2\chi}{d\xi^2} - \omega\frac{d\chi}{d\xi} - \ell\chi = -se^{\alpha\xi} \tag{35}$$

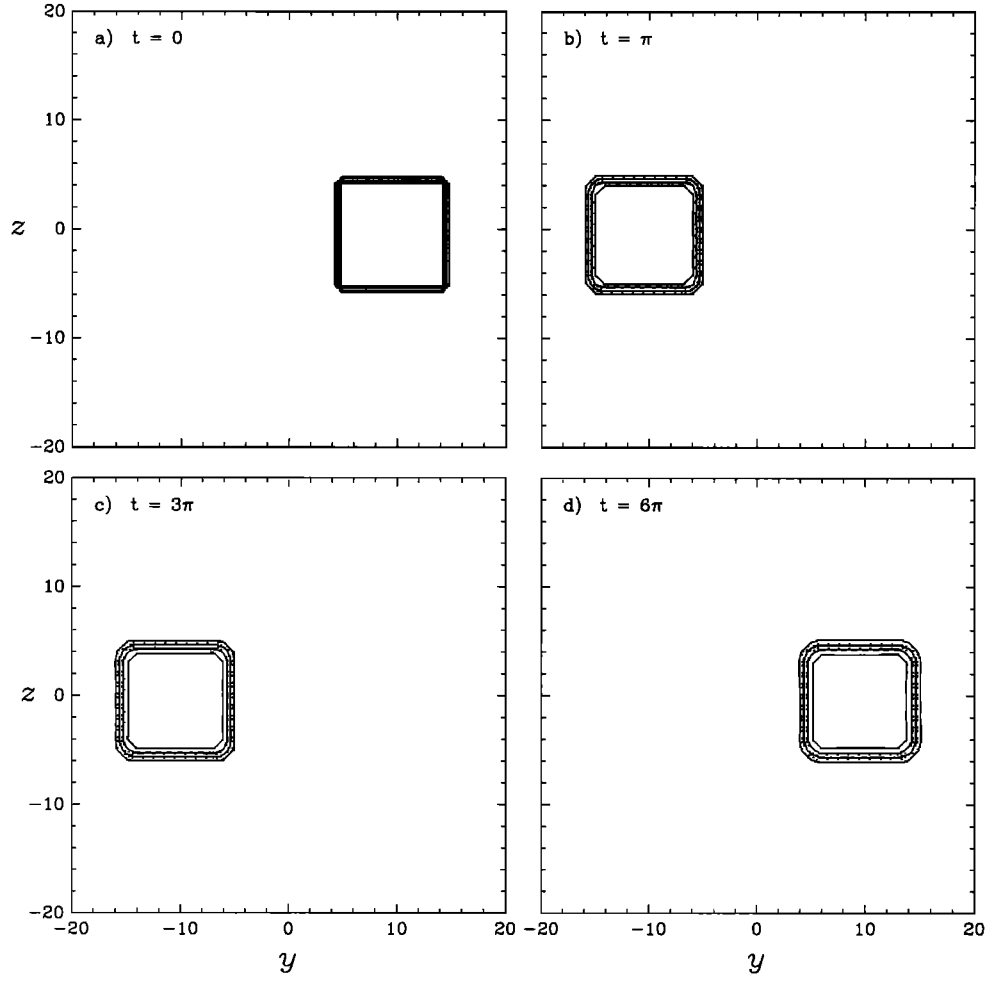

Fig. 4. Same as Figure 2, with a square column as initial condition. The contour lines represent concentrations 0.2, 0.4, 0.6, and 0.8, respectively, from the outside to the inside.

This is a second-order ordinary differential equation with constant coefficients. The solution can be readily obtained:

$$\chi(\xi) = c_1 e^{\mu_1 \xi} + c_2 e^{\mu_2 \xi} + c_3 e^{\alpha \xi} \tag{36}$$

where

$$\mu_1 = \frac{1}{2}\left\{\omega + \left(\omega^2 + 4\ell\right)^{\frac{1}{2}}\right\} \tag{37}$$

$$\mu_2 = \frac{1}{2}\left\{\omega - \left(\omega^2 + 4\ell\right)^{\frac{1}{2}}\right\} \tag{38}$$

$$c_3 = \frac{s}{\ell + \omega\alpha - \alpha^2} \tag{39}$$

and c_1 and c_2 are unknown coefficients to be determined by boundary conditions. Three experiments were designed to numerically simulate this solution. The relevant parameters are summarized in Table 2. The lower boundary is at $\xi = 0$, where we imposed a fixed mixing ratio of 1×10^{-9}. The upper boundary is at $\xi = 2$, where an escape velocity $v_1 = 600$ cm s^{-1} was applied (flux $= n_1 v_1$). The initial distribution of the tracer was set to zero, except at the lower boundary. The two-dimensional model was run in the "one-dimensional" mode. In the first experiment the tracer distribution was primarily controlled by advection. The resulting comparison between the analytic solution and the numerical solution at "steady state" ($t = 10^6$ s) is given in Figure 8*a*. The maximum error is 2%. Experiment 3b is the same as experiment 3a, except that $K_o = 2.56 \times 10^8$ cm^2 s^{-1} and $w_o = 80$ cm s^{-1}. The purpose of this experiment is to explore a regime where the tracer distribution is dominated by diffusion. The results are shown in Figure 8*b*. The maximum error is 0.5%. Experiment 3c is the same as experiment 3a, except that $L_o = 4 \times 10^{-4}$ s^{-1} and $w_o = 80$ cm s^{-1}. In this case the tracer distribution is determined mainly by chemistry. The results are shown in Figure 8*c*. The maximum error is 1.6%. It can be seen from Figures 8*a* through 8*c* that a satisfactory agreement between the analytic and numerical solution has been achieved.

Because this experiment incorporates all three processes in the model, advection, diffusion, and chemistry, we can investigate the effect of interchanging the order of computing these processes (see, for example, *McRae et al.* [1982]). We found that chemistry is least sensitive to the ordering, but computing diffusion before advection produces better results. In the worst case, reversing the order of computing diffusion and advection can produce as much as 15% error (at the boundary).

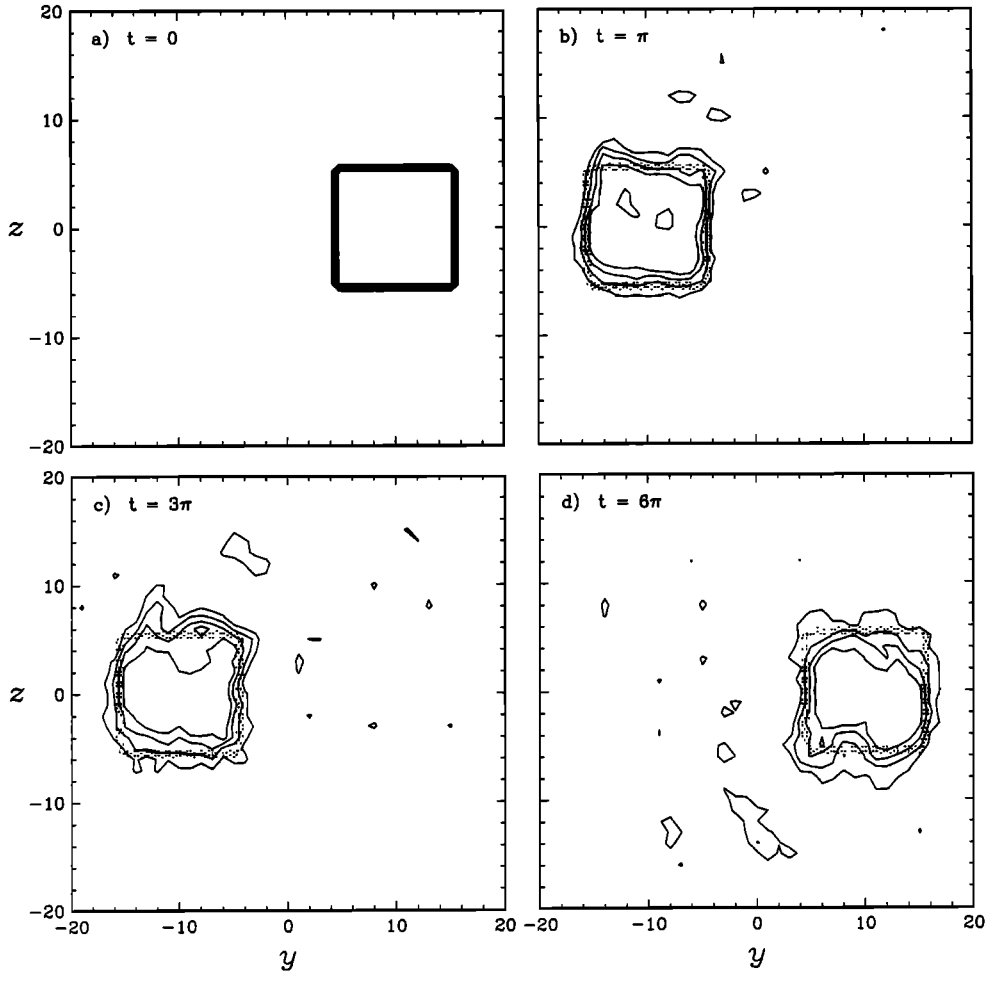

Fig. 5. Same as Figure 4, using Arakawa's scheme.

EXPERIMENT 4: ADVECTION IN TWO DIMENSIONS WITH CHEMISTRY

The previous experiments with Prather's method used a Cartesian grid. Here we test the method in a spherical atmosphere with pure advection and chemistry. *Prather's* [1986] original scheme was derived for a Cartesian grid. The formulation in a spherical atmosphere using $\xi - \theta$ grid is implicit in Prather's work. Here we provide the explicit formulas. The volume element of a grid box is now (see Figure 1),

$$\Delta V = Ha\, e^{-\xi} \cos\theta\, \Delta\theta\, \Delta\xi \tag{40}$$

where $\Delta\theta$ and $\Delta\xi$ denote the horizontal and vertical length of the grid box, respectively. The horizontal and vertical scaling factors for material fluxes are $He^{-\xi}\Delta\xi \cos\theta$ and $ae^{-\xi}\Delta\theta \cos\theta$, respectively. The accuracy of Prather's method in this new geometry with chemistry will be tested against an analytic solution.

Consider the simple stream function

$$\psi(y,z) = -w_o a \xi e^{\xi} (\cos\theta)^n \tag{41}$$

where n is a positive integer. The corresponding velocities can be computed using (1) and (2),

$$v(y,z) = \frac{w_o a}{H} e^{\xi} (\cos\theta)^{n-1} \tag{42}$$

$$w(y,z) = n w_o \xi e^{\xi} \sin\theta (\cos\theta)^{n-2} \tag{43}$$

The steady state continuity equation is, from (6),

$$\frac{w_o e^{\xi}}{H} (\cos\theta)^{n-1} \frac{\partial \chi}{\partial \theta} + \frac{n w_o}{H} \xi e^{\xi} \sin\theta (\cos\theta)^{n-2} \frac{\partial \chi}{\partial \xi} = \frac{1}{M}(P - L) \tag{44}$$

Dividing both sides of (44) by $(w_o/H)e^{\xi}\sin\theta(\cos\theta)^{n-2}$, we have

$$\frac{\cos\theta}{\sin\theta}\frac{\partial \chi}{\partial \theta} + n\xi \frac{\partial \chi}{\partial \xi} = \frac{He^{-\xi}}{w_o M} \frac{1}{\sin\theta(\cos\theta)^{n-2}} (P - L) \tag{45}$$

In order to derive an analytic solution to (45), we have to make a specific choice of P and L,

$$P = s \frac{w_o M_o}{H} \xi^{-\ell/n} \sin\theta (\cos\theta)^{n-2} \tag{46}$$

where s is a constant, and

$$L = \ell \frac{w_o}{H} M_o \sin\theta (\cos\theta)^{n-2} \chi \tag{47}$$

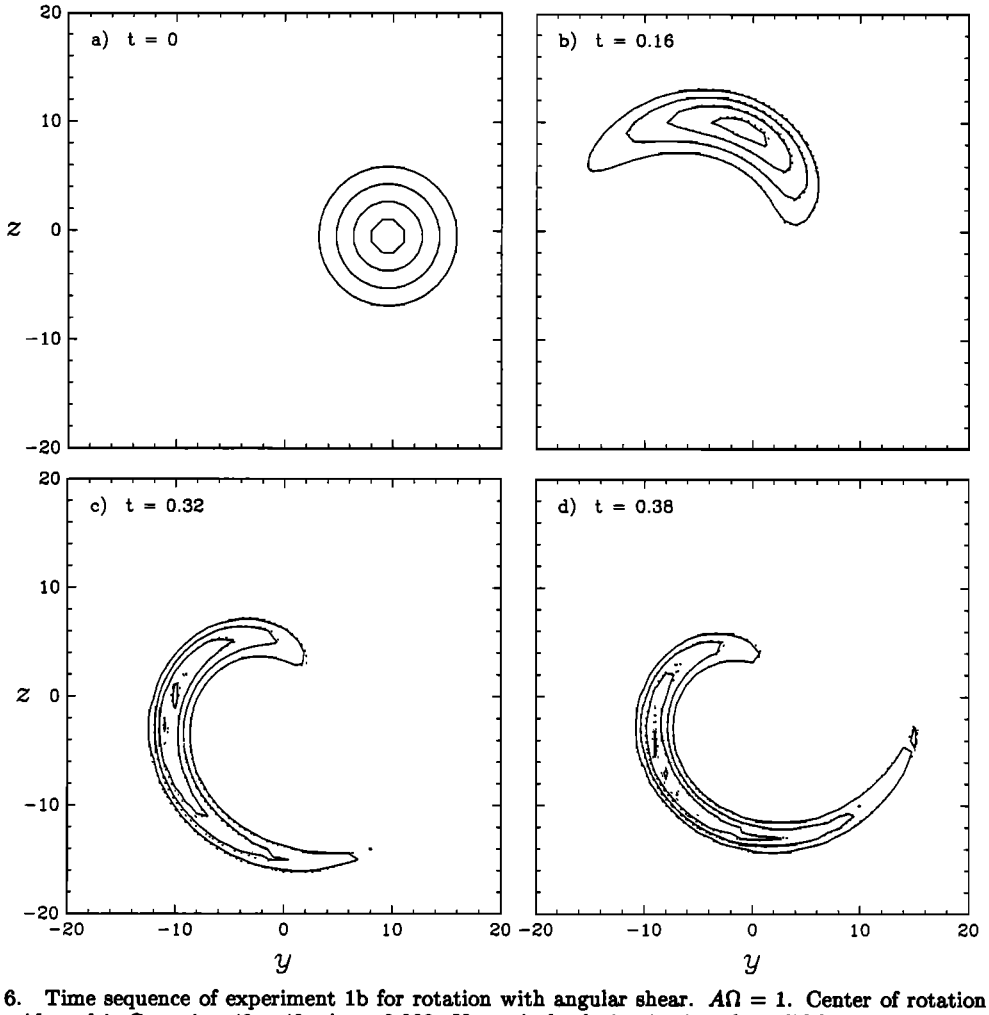

Fig. 6. Time sequence of experiment 1b for rotation with angular shear. $A\Omega = 1$. Center of rotation is $(0, 0)$. The grid used is Cartesian 40×40. $\Delta t = 0.002$. Numerical solution is given by solid lines; analytic solution by dotted lines. The algorithm used for computing advection is Prather's scheme.

where ℓ is a constant. This choice creates a somewhat unphysical situation in which P and L can be negative quantities. However, mathematically (and hence numerically) the problem is still well posed. With these assumptions, (45) becomes

$$\frac{\cos\theta}{\sin\theta}\frac{\partial\chi}{\partial\theta} + n\xi\frac{\partial\chi}{\partial\xi} = s\xi^{-\ell/n} - \ell\chi \tag{48}$$

Defining a set of new variables,

$$f = \xi^{\ell/n}\chi \tag{49}$$

$$\lambda = \ln(\cos\theta) \tag{50}$$

$$\varsigma = \frac{1}{n}\ln(\xi) \tag{51}$$

we obtain, from (48),

$$-\frac{\partial f}{\partial\lambda} + \frac{\partial f}{\partial\varsigma} = s \tag{52}$$

Equation (52) can be easily solved, and the answer is

$$f(\lambda, \varsigma) = s\varsigma + G(\lambda + \varsigma) \tag{53}$$

where G is to be determined by boundary conditions. Thus the analytic solution for the mixing ratio is

$$\chi(y, z) = \xi^{-\ell/n}\left\{\frac{s}{n}\ln(\xi) + G\left(\ln(\cos\theta) + \frac{1}{n}\ln\xi\right)\right\} \tag{54}$$

Note that the solution is symmetric in θ.

In order to test our model against this analytic solution, we make the following choice of parameters: $n = 2$, $a = 6372$ km, $H = 8$ km, $M_o = 8 \times 10^{16}$ cm^{-3}, $w_o = 80$ cm s^{-1}, $\ell = 6$, and $s = 1 \times 10^{-11}$. The function G in (54) is given by

$$G(x) = 2 \times 10^{-11}\left(1 + \frac{3}{10}e^x\right) \tag{55}$$

The lower and upper boundaries are at $\xi = 1$ and $\xi = 2$, respectively ($\xi = 0$ is avoided because the analytic solution has a singularity there). Figure 9*a* shows the mass-weighted stream function,

$$\Psi(y, z) = -e^{-\xi}\psi(y, z) = -w_o a\xi(\cos\theta)^2 \tag{56}$$

The horizontal and vertical velocities computed from (42) and (43) are given in Figures 9*b* and 9*c*, respectively. The two-dimensional model was run with a 19×17 grid with the following boundary conditions:

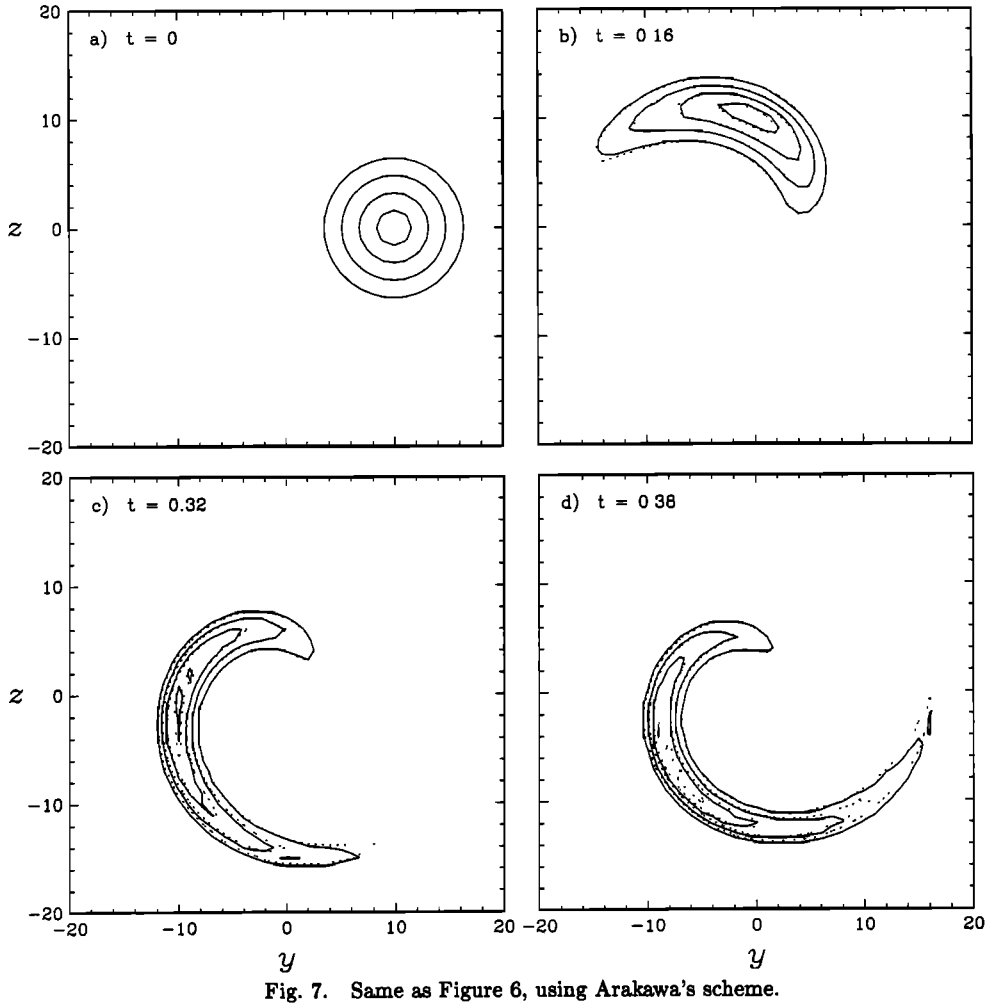

Fig. 7. Same as Figure 6, using Arakawa's scheme.

TABLE 2. Parameters and Coefficients Used in Generating Analytic Solutions for Experiments 3a, 3b, and 3c

	Case		
	3a	3b	3c
K_o, cm^{2}s^{-1}	6.4×10^7	2.56×10^8	6.4×10^7
w_o, cm s^{-1}	320	80	80
P_o, cm^{-3}s^{-1}	1×10^2	1×10^2	1×10^2
α	0.5	0.5	0.5
L_o, s^{-1}	1×10^{-4}	1×10^{-4}	4×10^{-4}
ω	4.0	0.25	1.0
s	1.25×10^{-11}	3.125×10^{-12}	1.25×10^{-11}
ℓ	1.0	0.25	4.0
μ_1	4.236	0.640	2.562
μ_2	-0.236	-0.390	-1.562
c_1	3.39×10^{-13}	5.55×10^{-11}	1.47×10^{-13}
c_2	9.95×10^{-10}	9.20×10^{-10}	9.97×10^{-10}
c_3	4.55×10^{-12}	2.50×10^{-11}	2.94×10^{-12}

The boundary conditions are $\chi(0) = 1.0 \times 10^{-9}$ at the lower boundary and $\phi_1 = n_1 v_1$ at the upper boundary, where ϕ_1 is flux, n_1 is number density at the upper boundary, and v_1 =is 600 cm s^{-1}.

$$\chi(\theta, \xi = 1) = 2 \times 10^{-11}\left(1 + \frac{3}{10}\cos\theta\right)$$

$$\chi(\theta, \xi = 2) = 2.5 \times 10^{-12}\left(1 + \frac{1}{4}\ln 2 + \frac{3\sqrt{2}}{10}\cos\theta\right) \quad (57)$$

The initial condition chosen was zero concentration everywhere, except for the boundaries, as stated above. A "steady state" solution was achieved after 10^6 s model time. The results for the model and the exact solution are shown in Figure 9*d*. The maximum error occurs in the lower left corner of this figure, but does not exceed 2.5%. Hence we conclude that the accuracy achieved by Prather's method in this problem is sufficient.

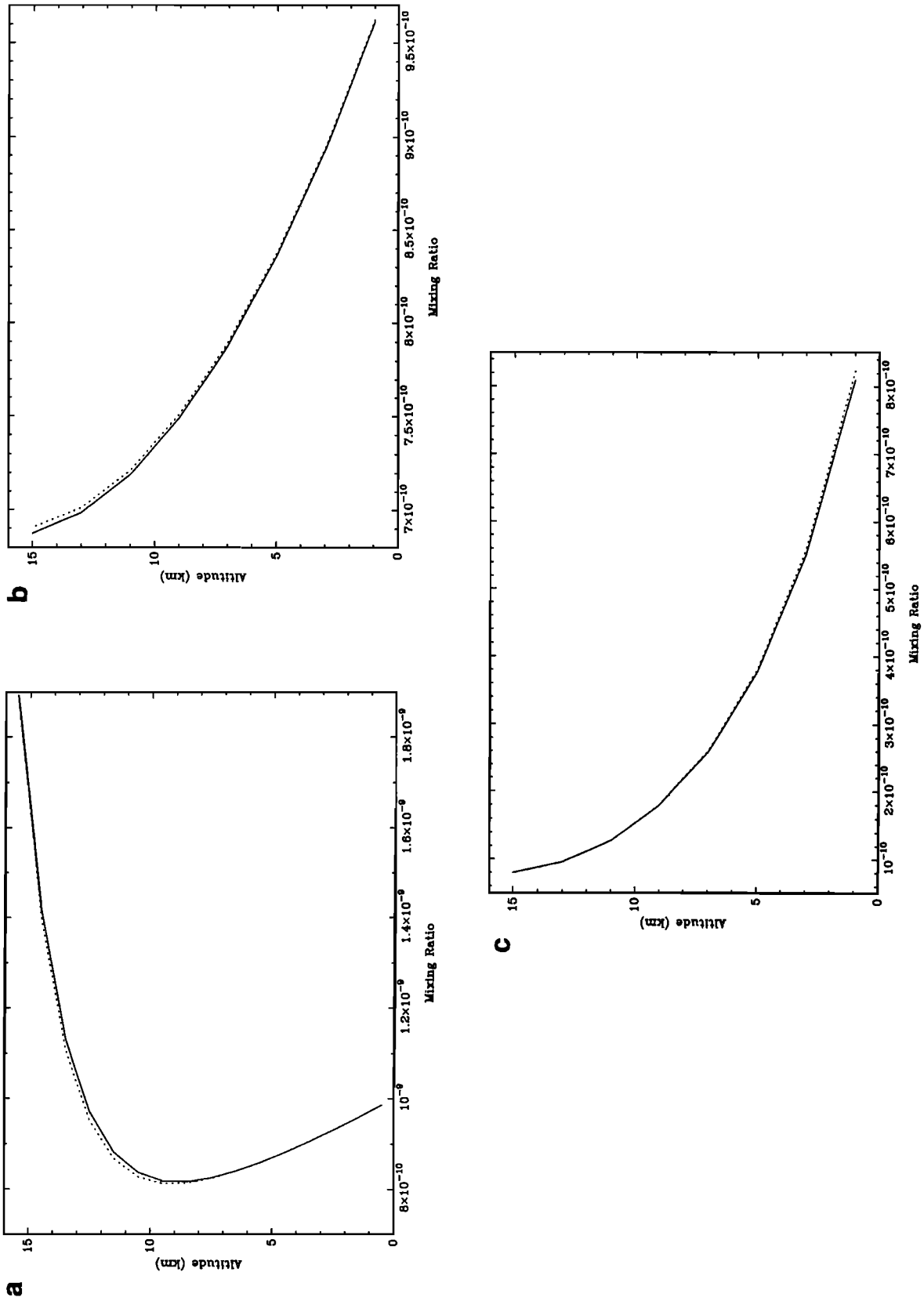

Fig. 8. (*a*) Simulation of the one-dimensional continuity equation with flow using Prather's method for advection and finite difference method for diffusion, for numerical experiment 3a. The parameters relevant to this run are summarized in Table 2. Solid curve, numerical solution; dotted curve, analytic solution. The maximum error is 2%. (*b*) Same as Figure 8*a*, except $K_o = 2.56 \times 10^8$ cm^2 s^{-1} and $w_o = 80$ cm s^{-1}. This is numerical experiment 3b. The maximum error is 0.5%. (*c*) Same as Figure 8*a*, except $w_o = 80$ cm s^{-1} and $L_o = 4 \times 10^{-4}$ s^{-1}. This is numerical experiment 3c. The maximum error is 1.6%.

EXPERIMENT 5: A MORE REALISTIC ADVECTION

The stream functions used in experiments 1–4 bear little resemblance to the atmospheric circulation. A more stringent test was proposed by R. Rood (private communication, 1989). The circulation is represented by horizontal and vertical velocity fields

$$v = 10H\cos\theta\left[\frac{\pi}{z_t}\cos\left(\pi\frac{z}{z_t}\right) - \frac{1}{H}\sin\left(\pi\frac{z}{z_t}\right)\right] \tag{58}$$

$$w = 20\frac{H}{a}\sin\theta\sin\left(\pi\frac{z}{z_t}\right) \tag{59}$$

where $H = 7$ km is the scale height, $z_t = 93.75$ km, θ is the latitude ($-90° \le \theta \le 90°$), and z is the altitude ($0 \le z \le z_t$). These velocity fields can be derived from the following stream function:

$$\psi = -10H\cos^2\theta\sin\left(\pi\frac{z}{z_t}\right) \tag{60}$$

In Figure 10, solid curves represent the streamlines of the circulation in the $\theta - z$ plane produced by the stream function.

We used a 30×25 grid to simulate the transport of a tracer by this stream function. The first test case was a tracer with constant initial mixing ratio. The time step we used was very close to the Courant limit ($\Delta t = 0.9984$ Courant limit). After 2000 steps the mixing ratio of the tracer was exactly the same as the initial value everywhere.

Because we cannot find a nontrivial analytic solution for the transport equation with this circulation, the only analytic expression left to be compared with was the stream function itself. From Figure 10 it is easy to see that the circulation looks like a deformed rotation, with a fixed center and a set of closed streamlines around it. So if we keep the mixing ratio of the left half of the horizontal layer fixed all the time, the distribution of the mixing ratio would be constant along the streamline once the steady state is reached. The location of the fixed center is $\theta \sim 0$ and $z \sim 8.2$ km. The initial distribution of the mixing ratio in the second test case is

$$\chi_{ij}(t=0) = 0 \qquad \begin{matrix} 1 \le i \le 30 \\ 1 \le j \le 25 \end{matrix}$$

and the fixed values on the left half strip are

$$\chi_{ij}(t>0) = 0.01 \times i \qquad \begin{matrix} 1 \le i \le 15 \\ j = 3 \end{matrix}$$

In Figure 10 the dashed curves are the contours of constant mixing ratio after 2000 steps. Those dashed curves are very close to the streamlines which are represented by solid curves in Figure 10. By contrast, although the fourth-order Arakawa algorithm passed the test with constant initial distribution, it totally failed the second test. We used a time step 12 times smaller in the Arakawa scheme than the one used in the Prather algorithm and calculated in rectangular coordinates, which should be simpler than in spherical coordinates. But the numerical dispersion produced a large amount of negative numbers for the mixing ratio, and the results become meaningless after several hundred time steps. The Prather algorithm gave a result similar to that shown in Figure 10 in the rectangular coordinates. So this experiment clearly demonstrates that the Prather algorithm is superior to the Arakawa algorithm for a quite realistic stream function.

EXPERIMENT 6: EXTENSION TO THIRD- AND FOURTH-ORDER MOMENTS

From Table 2 of *Prather* [1986], it is obvious that the accuracy of the advection algorithm has increased tremendously by including higher-order moments. Prather stopped at second-order moments in his paper. Naturally, it is tempting to extend his method to higher orders. A potential advantage of higher-order schemes is the use of coarser grids. This would allow running the model with larger time steps. Prather listed all formulas for second moments in the paper. An extension of his method requires formulas for higher-order moments, a tedious mechanical task. There is a symbolic manipulation program designed for an IBM-PC that is suitable for this. A sample of the coefficients for the fourth-order method is listed in Appendix C.

The second-order method already gives very accurate numerical results when the grid spacing is small. Hence the advantage of using higher moments methods is realized only in cases with coarse grids. We tested third- and fourth-order moment methods in one dimensional advection, using the following initial distribution (see Figure 11*a*):

$$\begin{matrix} f(x) = Ax^4 + Bx^3 + Cx^2 + Dx + E & 0 \le x \le 20 \\ f(x) = 0 & 20 < x \le 40 \end{matrix} \tag{61}$$

where $A = -7/1500$, $B = 1/6$, $C = -19/12$, $D = 7/3$, and $E = 50$. In three experiments, the region $0 \le x \le 40$ is divided into 40, 20, and 10 grid points, respectively, and the periodic boundary condition is imposed. We chose the time step

$$\Delta t = \frac{1}{2}\Delta t_{\max} \tag{62}$$

where

$$\Delta t_{\max} = \frac{\Delta x}{V} \tag{63}$$

is the Courant limit corresponding to the velocity V. In Figures 11*b* through 11*d* the numerical results of the distribution after 480 time steps are shown using second-, third-, and fourth- order moments methods along with the analytic solution. In the case of fine resolution (40 grid boxes), the improvement in accuracy is not significant mainly because the original Prather scheme is already extremely accurate. However, for cases with coarser resolution (20 and 10 grid boxes), there is substantial improvement. Figures 11*c* and 11*d* show that the maximum difference occurs at the endpoints, $x = 0$ and 40, and at the midpoint $x = 20$. The details of these computations are summarized in Table 3. This table has been constructed by analogy with Table 2 of *Prather* [1986], and the reader is referred to that paper for a detailed explanation of the contents of Table 3. In practice, coarser resolution may not be very useful if we want to model atmospheric phenomena with small length scales (such as the Antarctic ozone depletion).

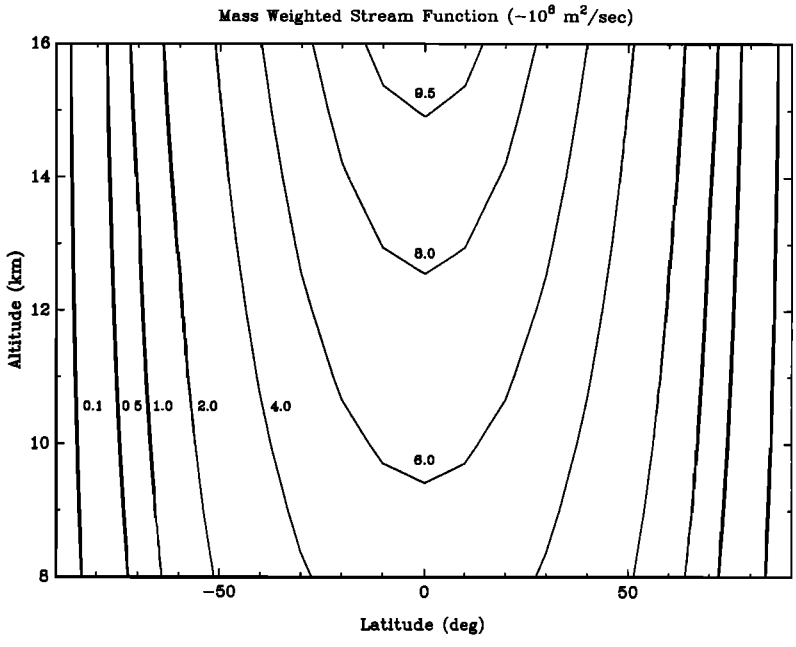

Fig. 9*a*. Mass-weighted stream function as defined by equation (56) in units of -10^6 m^2 s^{-1}.

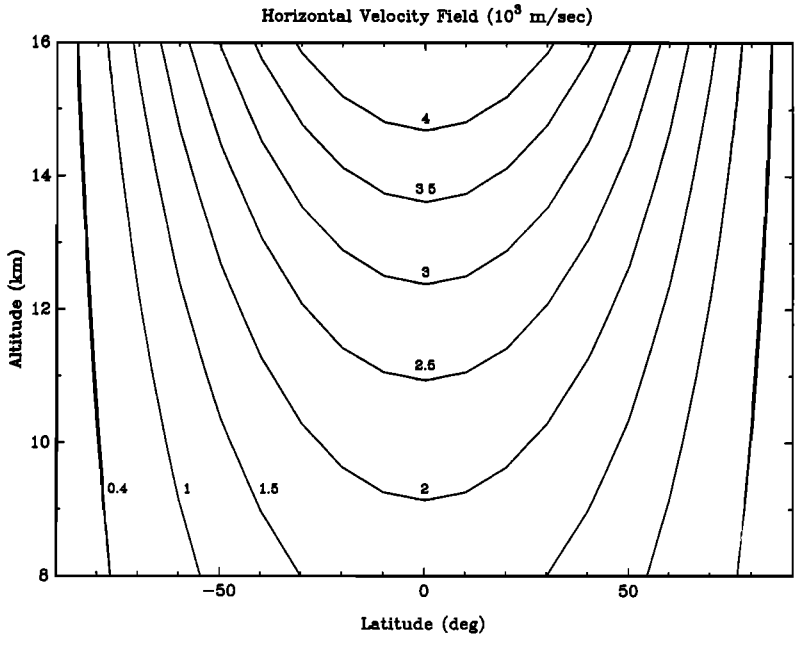

Fig. 9*b*. Horizontal velocity v (10^3 m s^{-1}) derived from the stream function given in Figure 9*a*.

In the experiments with fourth-order moments, all moments were set to their exact values at $t = 0$. We repeated the experiments with the following initial conditions to test the sensitivity of the results to initial moment distributions: in case a, only the zeroth moment was exact, and all others were zero; in case b, only the first two moments were exact, and all others were zero. In cases c and d only the first three and first four moments were exact, and all other moments were zero. The results show that case a has large errors, but cases b–d give almost the same answers as the original case with all initial moments exactly prescribed. Therefore we conclude that as far as initial conditions are concerned, only the first two moments are important, at least for this case we studied in detail.

CONCLUSIONS

We have modified and extended Prather's method of advection to a spherical atmosphere, higher orders, and in combination with eddy diffusion and chemistry. Six numerical experiments have been performed to test the adequacy of the scheme for our two-dimensional model for tracers. Experiments 1 and 2 showed that Prather's scheme faithfully preserved the morphology of contour lines under two kinds of rotational motion: constant angular velocity and constant angular shear. Experiment 3 demonstrated that the scheme performed well in the presence of eddy diffusion and chemistry in one dimension. Experiment 4 involves pure

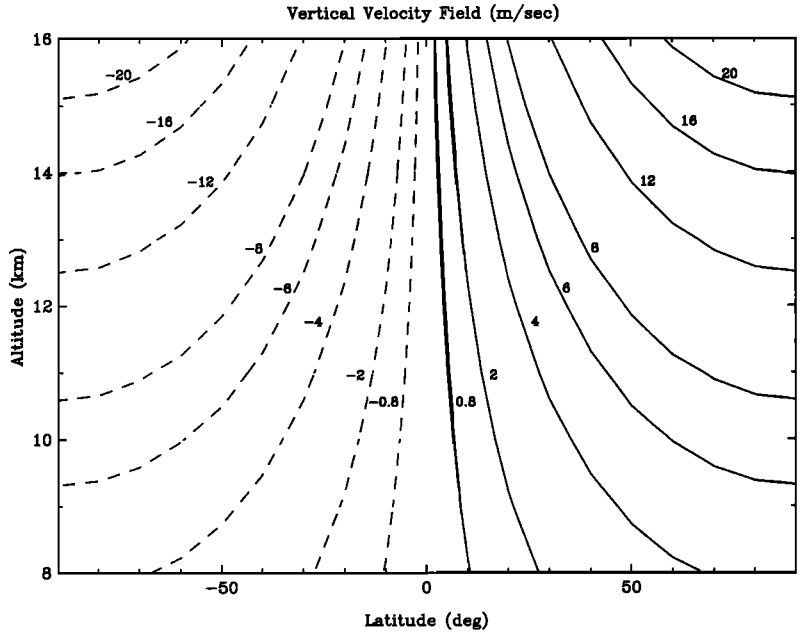

Fig. 9c. Vertical velocity w (m s^{-1}) derived from the stream function given in Figure 9a.

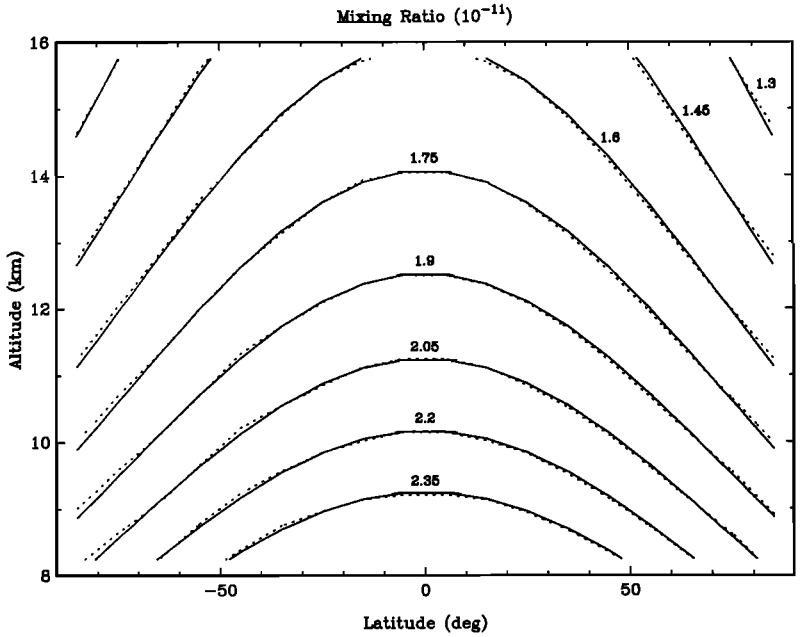

Fig. 9d. Comparison of computed mixing ratio (experiment 4) and that given by the exact solution. The units are 1×10^{-11}. Solid curve, numerical solution; dotted curve, analytic solution. The maximum error is 2.5%.

advection with chemistry in a spherical atmosphere in two dimensions. Again the new method was shown to be highly accurate. However, experiments 3 and 4 do not provide the most stringent tests of Prather's scheme. The results of these experiments could be duplicated by fourth-order finite difference schemes (R. Rood, private communication, 1989). A more realistic circulation has been used in experiment 5. In this rather difficult simulation the performance of the Prather scheme remains satisfactory, while the fourth-order Arakawa scheme fails catastrophically. The Prather scheme can be readily generalized to include conservation of third- and fourth-order moments as shown in experiment 6.

Having performed these numerical experiments and comparing the results with analytic solutions, we conclude that Prather's method with conservation of second-order moments is robust, has practically no numerical diffusion, and can preserve discontinuities, and sharp gradients of concentration profiles. In all tests performed in this work, emphasis is placed on comparisons with steady state analytic solutions. Thus we have largely ignored testing the time dependent aspect of the Prather scheme. It is hoped that in the future, time dependent analytic solutions to (6) will be discovered so that tests similar to those described in this paper can be carried out.

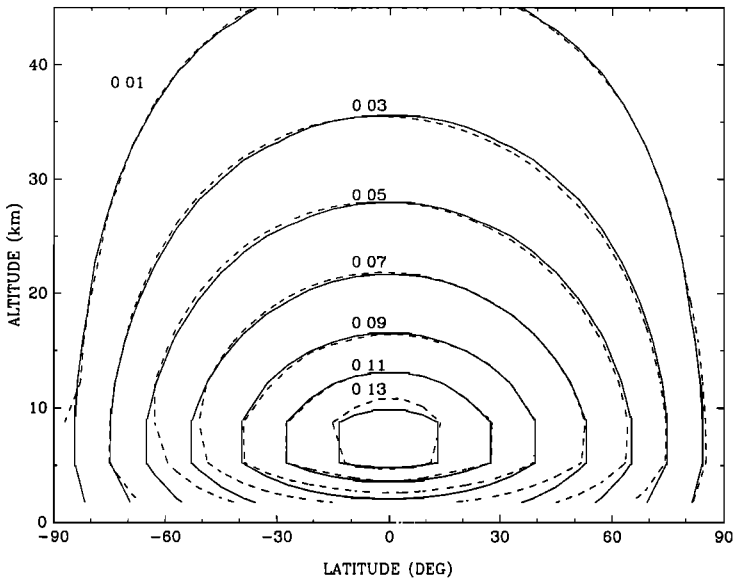

Fig. 10. Results of experiment 5. Solid curves, exact solution; dashed curves, numerical solution after 2000 steps.

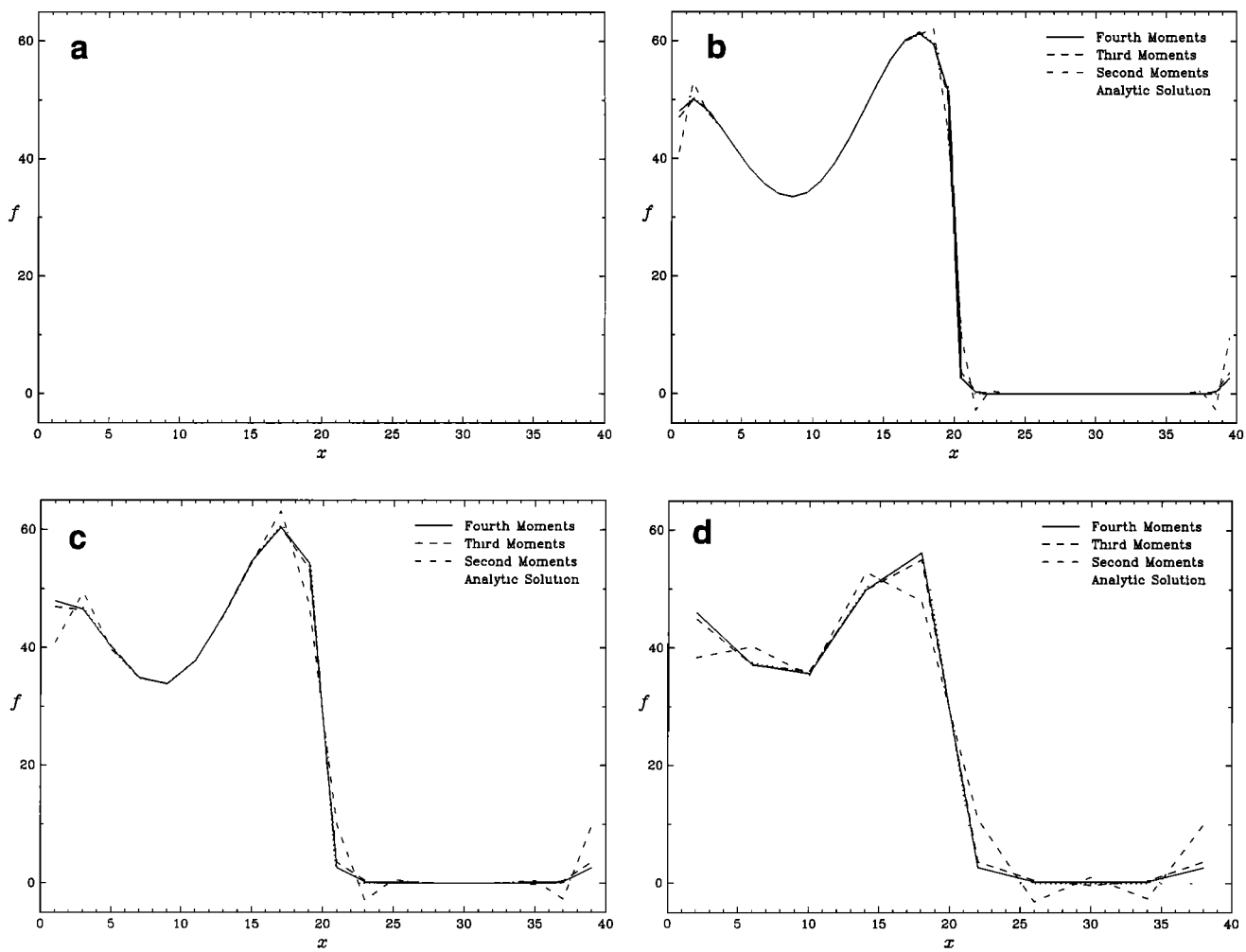

Fig. 11. (*a*) Initial tracer distribution used in numerical experiment 6. (*b*) Tracer distributions after 480 steps with $\Delta t = \frac{1}{2}\Delta x/V$ using Prather's scheme for advection with conservation of second-, third-, and fourth-order moments. The computations were carried out using 40 grid boxes. (*c*) Same as Figure 11*b*, using 20 grid boxes. (*d*) Same as Figure 11*b*, using 10 grid boxes.

TABLE 3. Comparison of Accuracy of Prather's Scheme for Advection Using Conservation of Second-, Third-, and Fourth-Order Moments

Grid Resolution	Moments Conserved	Number of Steps	$\frac{\sum f_j^2(t)}{\sum f_j^2(0)}$	$\frac{\sum\lvert f_j(t)-f_j(0)\rvert}{\text{Grid Resolution}}$	$\max\lvert f_j(t)-f_j(0)\rvert$
40	initial distribution	0	1	0	0
40	fourth	480	0.9862	0.3036	2.6407
40	third	480	0.9828	0.4212	3.6429
40	second	480	0.9743	1.2865	9.6290
20	initial distribution	0	1	0	0
20	fourth	480	0.9719	0.6091	2.6539
20	third	480	0.9643	0.8476	3.7023
20	second	480	0.9455	2.6124	9.9721
10	initial distribution	0	1	0	0
10	fourth	480	0.9445	1.2310	2.7017
10	third	480	0.9274	1.7316	3.8793
10	second	480	0.8766	5.4592	10.8616

APPENDIX A: MASS CONSERVATION

Local mass conservation in our model is achieved by defining the stream function at the corners of the grid box. There is no need for any further adjustment of the velocity field. Consider the total mass flow into a box, with corners defined by (i,j), $(i+1,j)$, $(i,j+1)$, and $(i+1,j+1)$ (see Figure 1). The horizontal mass flow is

$$\Phi_y = \rho v \Delta S_y \tag{A1}$$

and the vertical mass flow is

$$\Phi_z = \rho w \Delta S_z \tag{A2}$$

where

$$\rho = \rho_o e^{-\xi} \tag{A3}$$

is the density of the ambient atmosphere; v and w are the meridional and vertical velocity, respectively, and

$$\Delta S_y = 2\pi a \cos\theta \Delta z \tag{A4}$$

$$\Delta S_z = 2\pi a \cos\theta \Delta y \tag{A5}$$

are the side areas of the grid box. The factor $2\pi a\cos\theta$ comes from the integration along the longitude.

The usual centered finite difference procedure gives

$$(\Phi_y)_{i,j+1/2} = \rho_{j+1/2}\, v_{i,j+1/2} (\Delta S_y)_{i,j+1/2} \tag{A6}$$

where

$$\rho_{j+1/2} = \rho_o e^{-\xi_{j+1/2}} \tag{A7a}$$

$$v_{i,j+1/2} = -\frac{1}{\cos\theta_i} e^{\xi_{j+1/2}} \frac{1}{(\Delta Z)_{j+1/2}} \times \left(e^{-\xi_{j+1}}\psi_{i,j+1} - e^{-\xi_j}\psi_{i,j}\right) \tag{A7b}$$

$$(\Delta S_y)_{i,j+1/2} = 2\pi a \cos\theta_i (\Delta Z)_{j+1/2} \tag{A7c}$$

To derive (A7), equation (1) has been used. Combining (A6) and (A7), we find

$$(\Phi_y)_{i,j+1/2} = 2\pi a \rho_o \left(e^{-\xi_{j+1}}\Phi_{i,j+1} - e^{-\xi_j}\Phi_{i,j}\right) \tag{A8}$$

Similarly, the vertical mass flow is

$$(\Phi_z)_{i+1/2,j} = \rho_j w_{i+1/2,j} (\Delta S_z)_{i+1/2,j} \tag{A9}$$

where

$$\rho_j = \rho_o e^{-\xi_j} \tag{A10a}$$

$$w_{i+1/2,j} = \frac{1}{\cos\theta_{i+1/2}} \frac{1}{(\Delta Y)_{i+1/2}} (\psi_{i+1,j} - \psi_{i,j}) \tag{A10b}$$

$$(\Delta S_z)_{i+1/2,j} = 2\pi a \cos\theta_{i+1/2} (\Delta Y)_{i+1/2} \tag{A10c}$$

and

$$(\Phi_z)_{i+1/2,j} = -2\pi a \rho_o \left(e^{-\xi_j}\psi_{i+1,j} - e^{-\xi_j}\psi_{i,j}\right) \tag{A11}$$

The total mass flow out of the grid box is

$$\begin{aligned}(\Phi_{\text{total}})_{i+1/2,j+1/2} &= (\Phi_y)_{i+1,j+1/2} - (\Phi_y)_{i,j+1/2} \\ &\quad + (\Phi_z)_{i+1/2,j+1} - (\Phi_z)_{i+1/2,j} \\ &= 2\pi a \rho_o \Big(e^{-\xi_{j+1}}\psi_{i+1,j+1} - e^{-\xi_j}\psi_{i+1,j} \\ &\quad - e^{-\xi_{j+1}}\psi_{i,j+1} + e^{-\xi_j}\psi_{i,j} \\ &\quad - e^{-\xi_{j+1}}\psi_{i+1,j+1} + e^{-\xi_{j+1}}\psi_{i,j+1} \\ &\quad + e^{-\xi_j}\psi_{i+1,j} - e^{-\xi_j}\psi_{i,j}\Big) = 0\end{aligned} \tag{A12}$$

Thus we have proven that for a velocity field $\mathbf{u} = (v,w)$, derived from a stream function ψ using (1) and (2), our advection scheme conserves mass in each grid box. Note that this proof is only for the flow of bulk mass of the atmosphere (the theorem is not true for tracer mass flow). In addition, the result holds for any other scheme which uses stream function as described here.

APPENDIX B: ARAKAWA METHOD

The equation for advection,

$$\frac{\partial \chi}{\partial t} + \mathbf{u}\cdot\nabla\chi = 0 \tag{B1}$$

where $\mathbf{u} = (v,w)$, can be written in the following form

$$\frac{\partial \chi}{\partial t} = \mathbf{J}(\psi,\chi) \tag{B2}$$

where the Jacobian is

$$\mathbf{J}(\psi,\chi) \equiv \begin{vmatrix} \frac{\partial\psi}{\partial y} & \frac{\partial\psi}{\partial z} \\ \frac{\partial\chi}{\partial y} & \frac{\partial\chi}{\partial z} \end{vmatrix} \tag{B3}$$

and the stream function ψ is related to the velocities by

$$v = \frac{\partial\psi}{\partial z} \tag{B4}$$

$$w = -\frac{\partial\psi}{\partial y} \tag{B5}$$

The operator $\mathbf{u}\cdot\nabla$ in (B1) is the vectorial form of the operation

$$\mathbf{u}\cdot\nabla \equiv \left(v\frac{\partial}{\partial y} + w\frac{\partial}{\partial z}\right) \tag{B6}$$

Arakawa [1966] devised an elegant fourth-order finite difference scheme

$$\mathbf{J}_{ij}(\psi,\chi) = \sum_{i',j'} a_{i,j;i',j'}\chi_{i',j'} \tag{B7}$$

which is stable for long-time integration.

To guarantee that the Jacobian J vanishes when the mixing ratio is a constant everywhere, we have

$$\sum_{i',j'} a_{i,j;i'j'} = 0 \tag{B8}$$

Also, the coefficients $a_{ij,i'j'}$ are antisymmetrical in the following sense (equation (20) in Arakawa's paper):

$$a_{i,j;i',j'} = -a_{i',j';i,j} \tag{B9}$$

From (B8) and (B9), we have

$$\sum_{i,j} a_{i,j;i'j'} = 0 \tag{B10}$$

When the semi-implicit time marching is used, (B2) and (B7) give the change of the mixing ratio,

$$\chi_{i,j}^{(n+1)} = \chi_{i,j}^{(n)} + \sum_{i',j'} a_{i,j;i',j'}\chi_{i',j'}^{(n+1/2)}\Delta t \tag{B11}$$

where

$$\chi_{i',j'}^{(n+1/2)} \equiv \frac{1}{2}\left[\chi_{i',j'}^{(n)} + \chi_{i',j'}^{(n+1)}\right] \tag{B12}$$

and the finite time difference,

$$\frac{\partial\chi}{\partial t} \approx \frac{\chi^{(n+1)} - \chi^{(n)}}{\Delta t} \tag{B13}$$

has been used with

$$\chi^{(n)} \equiv \chi(n\Delta t) \tag{B14}$$

The conservation of total tracer mass is proved using (B11) and (B10),

$$\sum_{i,j}\chi_{i,j}^{(n+1)} = \sum_{ij}\chi_{i,j}^{(n)} + \sum_{i,j}\sum_{i',j'} a_{i,j;i',j'}\chi_{i',j'}^{(n+1/2)}\Delta t = \sum_{ij}\chi_{i,j}^{(n)} \tag{B15}$$

Multiplying equation (B11) by $\chi_{i,j}^{(n+1/2)}$ and summing over indices i, j, we get

$$\sum_{i,j}\chi_{i,j}^{(n+1)}\chi_{i,j}^{(n+1/2)} = \sum_{i,j}\chi_{ij}^{(n)}\chi_{ij}^{(n+1/2)} + \sum_{i,j}\sum_{i',j'} a_{i,j;i',j'}\chi_{ij}^{(n+1/2)}\chi_{i'j'}^{(n+1/2)} = \sum_{ij}\chi_{ij}^{(n)}\chi_{ij}^{(n+1/2)} \tag{B16}$$

The antisymmetric character of $a_{i,j}$ (equation (B9)), has been used to find (B16). From (B16) we have the conservation of squared mass,

$$\sum_{i,j}\left(\chi_{i,j}^{(n+1)}\right)^2 = \sum_{i,j}\left(\chi_{i,j}^{(n)}\right)^2 \tag{B17}$$

using the definition of $\chi_{i,j}^{(n+1/2)}$ (equation (B12)).

APPENDIX C: SOME FORMULAS FOR FOURTH-ORDER MOMENT METHOD

Instead of equation (5) in Prather's paper, we have

$$\begin{aligned} f(x,y,z) = a_o &+ a_x x + a_{xx}x^2 + a_{xxx}x^3 + a_{xxxx}x^4 \\ &+ a_y y + a_{yy}y^2 + a_{yyy}y^3 + a_{yyyy}y^4 \\ &+ a_z z + a_{zz}z^2 + a_{zzz}z^3 + a_{zzzz}z^4 \\ &+ a_{xy}xy + a_{xxy}x^2y + a_{xxxy}x^3y \\ &+ a_{xz}xz + a_{xxz}x^2z + a_{xxxz}x^3z \\ &+ a_{yz}yz + a_{xyy}xy^2 + a_{xyyy}xy^3 \\ &\quad + a_{yyz}y^2z + a_{yyyz}y^3z \\ &\quad + a_{xzz}xz^2 + a_{xzzz}xz^3 \\ &\quad + a_{yzz}yz^2 + a_{yzzz}yz^3 \\ &\quad + a_{xyz}xyz + a_{xxyy}x^2y^2 \\ &\qquad + a_{xxzz}x^2z^2 \\ &\qquad + a_{yyzz}y^2z^2 \\ &\qquad + a_{xxyz}x^2yz \\ &\qquad + a_{xyyz}xy^2z \\ &\qquad + a_{xyzz}xyz^2 \end{aligned}$$

where a_o, a_x, a_y, $\cdots$ are constants. Instead of equation (9) in Prather's paper, we have

$$K_o = 1$$

$$K_x = \chi - \frac{X}{2}$$

$$K_{xx} = x^2 - Xx + \frac{X^2}{6}$$

$$K_{xxx} = x^3 - \frac{3}{2}Xx^2 + \frac{3}{5}X^2x - \frac{X^3}{20}$$

$$K_{xxxx} = x^4 - 2Xx^3 + \frac{9}{7}X^2x^2 - \frac{2}{7}X^3x + \frac{X^4}{70}$$

Similar expressions for $K_y \cdots K_{yyyy}$, and $K_z \cdots K_{zzzz}$

$$K_{xy} = K_x \cdot K_y$$

and similar for K_{yz}, K_{xz},

$$K_{xxy} = K_{xx} \cdot K_y$$

and similar for K_{yyz}, $K_{xzz} \cdots$,

$$K_{xyz} = K_x \cdot K_y \cdot K_z$$

$$K_{xxxy} = K_{xxx} \cdot K_y$$

and similar for K_{xxxz}, $\cdots$, K_{yzzz},

$$K_{xxyy} = K_{xx} \cdot K_{yy}$$

and similar for K_{xxzz}, K_{yyzz}

$$K_{xxyz} = K_{xx} \cdot K_y \cdot K_z$$

and similar for K_{xyyz}, K_{xyzz}.

The following expressions for higher moments should be added into equation (11) in Prather's paper:

$$S_{xxx} = \left(\frac{350}{3X^3}\right) \int dv f(x, y, z) K_{xxx}(x)$$

$$S_{x^2yz} = \left(\frac{1080}{X^2YZ}\right) \int dv f(x, y, z) K_{xxyz}(x, y, z)$$

Accordingly, S_o^R in equation (19) in Prather's paper should become

$$S_o^R = \alpha \Big[S_o + (1-\alpha) S_x + (1-\alpha)(1-2\alpha) S_{xx} + \frac{6}{5}(1-\alpha)(1-5\alpha+5\alpha^2) S_{xxx} + \frac{12}{7}(1-\alpha)(1-2\alpha)(1-7\alpha+7\alpha^2) S_{xxxx} \Big]$$

and

$$S_{xxxx}^R = \alpha^5 S_{xxxx}$$

Acknowledgments. We are indebted to M. Allen, D. Crisp, and R. Zurek for critical comments on the manuscript. We thank M. Prather for sending us the detailed derivations of his numerical scheme, and D. Stevenson for directing us to find an analytic solution for experiment 4. Special thanks are due to one of the referees (R. Rood) for suggesting experiment 5 and for insightful comments. This work is supported by NASA grant NAGW-413 to the California Institute of Technology. Y.L.H. acknowledges the support of a Caltech SURF Fellowship in the summer of 1987. After our work had been completed, we learned that Douglass et al. (1989) successfully used Prather's method in their two-dimensional model. Division of Geological and Planetary Sciences, California Institute of Technology, Contribution 4599.

REFERENCES

Arakawa, A., Computational design for long-term numerical integration of the equation of fluid motion: Two-dimensional incompressible flows, 1, *J. Comput. Phys.*, *1*, 119–143, 1966. Douglass, A. R., C. H. Jackman, and R. S. Stolarski, Comparison of model results transporting the odd nitrogen family with results transporting separate odd nitrogen species, *J. Geophys. Res.*, *94*, 9862–9872, 1989.

Garcia, R. R., and S. Solomon, A numerical model of the zonally averaged dynamical and chemical structure of the middle atmosphere, *J. Geophys. Res.*, *88*, 1379–1400, 1983.

Guthrie, P. D., C. H. Jackman, J. R. Herman, and C. J. McQuillan, A diabatic circulation experiment in a two-dimensional photochemical model, *J. Geophys. Res.*, *89*, 9589–9602, 1984.

Haltiner, G. J., and R. T. Williams, *Numerical Prediction and Dynamic Meteorology*, John Wiley, 477 pp., New York, 1980.

Ko, M. K. W., K. K. Tung, D. K. Weisenstein, and N. D. Sze, A zonal mean model of stratospheric tracer transport in isentropic coordinates: Numerical simulations for nitrous oxide and nitric acid, *J. Geophys. Res.*, *90*, 2313–2329, 1985.

Logan, J. A., M. J. Prather, S. C. Wofsy, and M. B. McElroy, Atmospheric chemistry: Response to human influence, *Philos. Trans. R. Soc. London, Ser. A*, *290*, 187–234, 1978.

Molenkamp, C. R., Accuracy of finite-difference methods applied to the advection equation, *J. Appl. Meteorol.*, *7*, 160–167, 1968.

McRae, G. J., W. R. Goodin, and J. H. Seinfeld, Numerical solution of the atmospheric diffusion equation for chemically reacting flows, *J. Comput. Phys.*, *45*, 1–42, 1982.

Prather, M. J., Numerical advection by conservation of second-order moments, *J. Geophys. Res.*, *91*, 6671–6681, 1986.

Rood, R. B., Numerical advection algorithms and their role in atmospheric transport and chemistry models, *Rev. Geophys.*, *25*, 71–100, 1987.

Tung, K. K., A coupled model of zonally averaged dynamics, radiation and chemistry, in *Transport Processes in the Middle Atmosphere*, edited by G. Visconti and R. Garcia, pp. 417–444, D. Reidel, Hingham, Mass., 1987.

Y. L. Ha, R.-L. Shia, J.-S. Wen, and Y. L. Yung, Division of Geological and Planetary Sciences, California Institute of Technology, Pasadena, CA 91125.

(Received June 6, 1988;
revised July 26, 1989;
accepted July 26, 1989.)